

Updated reach of CERN LHC and constraints from relic density, $b \rightarrow s\gamma$ and a_μ in the mSUGRA model

Howard Baer, Csaba Balázs, Alexander Belyaev*, Tadas Krupovnickas

Department of Physics, Florida State University

Tallahassee, FL 32306, USA

*E-mail: baer@hep.fsu.edu, balazs@hep.fsu.edu, belyaev@hep.fsu.edu,
tadas@hep.fsu.edu*

Xerxes Tata

Department of Physics and Astronomy, University of Hawaii,

Honolulu, HI 96822, USA

E-mail: tata@phys.hawaii.edu

ABSTRACT: We present an updated assessment of the reach of the CERN LHC pp collider for supersymmetric matter in the context of the minimal supergravity (mSUGRA) model. In addition to previously examined channels, we also include signals with an isolated photon or with a leptonically decaying Z boson. For an integrated luminosity of 100 fb^{-1} , values of $m_{1/2} \sim 1400 \text{ GeV}$ can be probed for small m_0 , corresponding to a gluino mass of $m_{\tilde{g}} \sim 3 \text{ TeV}$. For large m_0 , in the hyperbolic branch/focus point region, $m_{1/2} \sim 700 \text{ GeV}$ can be probed, corresponding to $m_{\tilde{g}} \sim 1800 \text{ GeV}$. We also map out parameter space regions preferred by the measured values of the dark matter relic density, the $b \rightarrow s\gamma$ decay rate, and the muon anomalous magnetic moment a_μ , and discuss how SUSY might reveal itself in these regions.

KEYWORDS: Supersymmetry Phenomenology, Supersymmetric Standard Model, Dark Matter.

*On leave of absence from Nuclear Physics Institute, Moscow State University.

1. Introduction

The search for supersymmetric (SUSY) matter is one of the primary objectives of experiments at high energy colliders[1]. SUSY matter may reveal itself through indirect effects[2], as in contributions to rare decays such as $b \rightarrow s\gamma$, $b \rightarrow s\ell\bar{\ell}$ or $B_s \rightarrow \mu^+\mu^-$, or via contributions to electric or magnetic moments such as the dipole electric moment of the electron or neutron or $(g-2)_\mu$. It is possible that relic SUSY cold dark matter (CDM) has already been detected gravitationally, and recent analyses of WMAP and other data sets indicate that the relic density $\Omega_{CDM}h^2 = 0.1126^{+0.0161}_{-0.0181}(2\sigma \text{ CL})$ [3], with a baryonic density about six times smaller. Both direct and indirect searches for relic SUSY CDM are underway[4]. Detection of a signal in any of these experiments would provide evidence for physics beyond the standard model, but the results may have both supersymmetric as well as non-supersymmetric interpretations.

The definitive discovery of SUSY matter will likely have to come from experiments operating at high energy colliders. Already, negative searches for SUSY by the LEP2 experiments have resulted in significant bounds: for instance, the light chargino \widetilde{W}_1 must have mass $m_{\widetilde{W}_1} > 103.5$ GeV[5], while a SM-like higgs boson must have mass $m_h > 114.1$ GeV[6]. The reach of the Fermilab Tevatron collider has been examined as well. In the context of the minimal supergravity model (mSUGRA)[7], with parameters

$$m_0, m_{1/2}, A_0, \tan \beta, \text{sign}(\mu), \quad (1.1)$$

$m_{1/2}$ values of up to 250 GeV (corresponding to $m_{\tilde{g}} \lesssim 600$ GeV) can be probed with 25 fb^{-1} for $m_0 \lesssim 200$ GeV[8] and small values of $\tan \beta$. Then, the best reach is obtained via the clean trilepton channel. The reach is considerably reduced for larger values of m_0 or for large values of $\tan \beta$ [9, 10, 11].

The CERN LHC is expected to begin operating in 2008 with pp collisions at $\sqrt{s} = 14$ TeV. While the initial luminosity is expected to be $\sim 10 \text{ fb}^{-1}$ per year, an integrated luminosity of several hundred fb^{-1} is ultimately anticipated. The reach of the LHC for supersymmetric matter has been evaluated in the mSUGRA model for low[12, 13, 14, 15] and high[16, 13, 14] values of $\tan \beta$, for slepton[17] and chargino-neutralino production[18], and even in the experimentally unfavorable case where the lightest supersymmetric particle (LSP) decays hadronically via R -parity violating interactions[19]. The LHC reach has also been evaluated for models with non-universal soft terms as given by non-minimal $SU(5)$ SUSY GUTs[20] and gaugino mediation models[21]. Finally, the LHC reach has been evaluated for gauge-mediated[22] (GMSB) and anomaly-mediated (AMSB) SUSY breaking models[23].

In studies evaluating the reach of the LHC, the signal channels have been classified by the number of isolated leptons present in each event. The isolated leptons usually arise as end products of cascade decays of gluinos, squarks or other massive SUSY particles[24]. At large values of the parameter $\tan \beta$, the b and τ Yukawa couplings become large, so that cascade decays to final states containing b -jets and τ -leptons are enhanced[25].

In this paper, we update our reach projections for the CERN LHC for several reasons.

- We calculate the sparticle production and cascade decay events using ISAJET v7.64[26]. This version includes a variety of radiative corrections and improvements to the sparticle mass spectrum that were not present in earlier ISAJET versions, including two-loop evolution of all RGEs. ISAJET 7.64 gives good agreement with spectra generated by the Suspect, SoftSUSY and Spheno codes, as compiled by Allanach, Kraml and Porod[27]. In addition, 3-body decay matrix elements are included[9, 28], so that decay product energy distributions are more accurately modeled.
- We adopt the code CMSJET v4.801 to model the CMS detector. This gives a more accurate portrayal of CMS than the toy detector models used in Ref. [12].
- We include additional channels to our reach projections, including events containing a reconstructed $Z \rightarrow \ell^+ \ell^-$ candidate ($\ell = e$ or μ)[29], and events containing isolated photons. The photonic events may arise from radiative neutralino decay[30, 31] $\tilde{Z}_2 \rightarrow \tilde{Z}_1 \gamma$ which is enhanced in the low μ [12] “hyperbolic branch” or “focus point” (HB/FP)[32, 33] region of parameter space.
- Our parameter space scans extend over a wider range than earlier reach projections. We are motivated to do so to cover the HB/FP region with small μ where SUSY phenomenology can be significantly different. Further, we adopt a higher integrated luminosity value of 100 fb^{-1} than our earlier studies; this integrated luminosity should be achieved after several years of LHC operation.
- We identify regions of mSUGRA parameter space consistent with recently updated constraints[2] from $b \rightarrow s\gamma$, $(g-2)_\mu$ and $\Omega_{\tilde{Z}_1} h^2$ calculations as well as the most recent constraints from the LEP2 experiments, and where there should be observable signals at the LHC.

In Sec. 2, we present the details of our computer calculations, cuts and detector simulation. In Sec. 3, we show our results for the LHC reach projections in the m_0 *vs.* $m_{1/2}$ plane, and identify parameter regions consistent with all experimental constraints. We summarize our results in Sec. 4.

2. Calculational details

We use the CMSJET (version 4.801) fast MC package[34] for the CMS detector response simulation. Both SM background and signal events were generated using ISAJET 7.64 which has undergone numerous upgrades since ISAJET 7.37 used in our last study[16]. The improvements include the incorporation of matrix elements for the calculation of three body decays of gluinos, charginos and neutralinos, two loop renormalization group evolution of all couplings and soft SUSY breaking parameters, inclusion of 1-loop self energies for third generation fermions, and improved evaluation of m_A which, in turn, significantly moves the boundary of the allowed parameter space of the mSUGRA model.

We have computed SM backgrounds from the following sources : $t\bar{t}$, QCD $2 \rightarrow 2$ including $c\bar{c}$ and $b\bar{b}$ production, $W + jets$ and $Z + jets$. Backgrounds from vector boson

pair production are negligible to the jetty signals that we consider in this study[12]. For the photonic signal we also included backgrounds from $W\gamma$ and $Z\gamma$ production, but found these to be negligible after hard cuts. Since the cross section of events with low p_T is much larger than that of events with high p_T , we generated the background events in several bins of p_T . We followed the division described in [13]. We have also adopted the cuts suggested in this study for E_T^{miss} , 0 lepton, 1 lepton, 2 OS and SS lepton, 3 lepton and ≥ 4 isolated lepton signals. We regard a lepton or a photon to be isolated if

- it has no charged particle with $p_T > 2$ GeV in a cone with $\Delta R < 0.3$ around the direction of the lepton.
- ΣE_T^{cell} in the region with $0.05 < \Delta R < 0.3$ around the lepton's direction has to be less than 10% of the lepton transverse energy.

For the convenience of the reader, we present these cuts in this paper. All events have to pass the following pre-cuts:

- $E_T^{miss} > 200$ GeV;
- Number of jets, $N_j \geq 2$.

We use a modified UA1-jetfinder routine GLOBJF, implemented in CMSJET, to identify calorimeter jets. A cluster of particles is labeled as a jet if it has transverse momentum p_T greater than 40 GeV and $|\eta| < 3$. Leptons are required to satisfy the following pre-cuts:

- $p_T > 10$ GeV for the muons, $p_T > 20$ GeV for the electrons, $|\eta| < 2.4$ for both muons and electrons.
- Electrons have to be isolated. Muon isolation is not required as part of the pre-cuts. We call an electron or muon non-isolated even if it satisfies the lepton isolation criteria but is part of a jet, or if it is isolated in the calorimeter, but non-isolated in the tracker. Naturally, if it is not isolated in the calorimeter then the lepton is called non-isolated.

The pre-cuts for the photons are:

- $p_T > 20$ GeV in $|\eta| < 2.4$.
- photons have to be isolated.

After events pass the pre-cuts, we impose 90% lepton detection efficiency for each lepton.

The events which pass the pre-cuts are divided into signal types according to the number of leptons (or photons for the isolated γ signal). In the case of the E_T^{miss} signal there can be any number of leptons, 0 lepton signal has no leptons, 1 lepton signal has 1 lepton, 2 OS lepton signal has 2 opposite sign leptons, 2 SS lepton signal has 2 same sign leptons, 3 lepton signal has 3 leptons, ≥ 4 lepton signal has more than 3 leptons, $Z \rightarrow \ell^+\ell^-$ signal has at least 2 OS, same flavor leptons with the invariant mass of this pair within the interval $(M_Z - \Delta M_Z, M_Z + \Delta M_Z)$ (ΔM_Z is varied during the optimization procedure).

Finally, the isolated γ signal has any number of leptons plus at least one photon (the cut on the number of photons is varied during the optimization procedure). Since muon isolation has not been included as part of the pre-cuts, if we impose the muon isolation during the optimization procedure, the number of events for some signal types can change.

A signal in any channel is considered to be observable if after our optimization procedure described below,

- the number of signal events $S \geq 10$ for an integrated luminosity of 100 fb^{-1} , and
- $S \geq 5\sqrt{B}$, where B is the corresponding number of background events.

We optimize the signal in each channel by imposing additional cuts. The set of cuts that we examined for this purpose are listed in Table 1. For the optimization of the signal $Z \rightarrow \ell^+ \ell^-$ signal, we have an additional cut: the invariant mass of the pair of opposite sign same flavor lepton pair has to be in the interval $(M_Z - \Delta M_Z, M_Z + \Delta M_Z)$ and ΔM_Z is taken to be $3, 6, 9, \dots, 30 \text{ GeV}$. For the case of the isolated photon signal, in addition to the optimization using the cuts in Table 1, we also vary the number of photons which can be $1, 2, 3, 4, \geq 5$. However, for large values of m_0 and $m_{1/2}$, events with $N_\gamma^{iso} > 1$ are generally too rare to pass the requirement of $S > 10$.

For each mSUGRA point that we analyze, we pass the various signals through each one of the complete set of cuts just discussed. If the signal satisfies our observability criterion for any one of these cut choices, we consider it to be observable.¹

Table 1: The set of cuts that we have examined for the optimization of the SUSY signal. Except for the muon isolation, the numbers refer to the lower bound on the quantity listed in the first column.

Variable(s)	Values
N_j	2, 3, 4, ..., 10
E_T^{miss}	200, 300, 400, ..., 1400 GeV
E_T^{j1}	40, 150, 300, 400, 500, 600, 700, 800, 900, 1000 GeV
E_T^{j2}	40, 80, 200, 200, 300, 300, 400, 400, 500, 500 GeV
$\Delta\phi (p_T^l, E_T^{miss})$	0, 20 deg.
<i>Circularity</i>	0, 0.2
μ isolation	on, off

3. Results

3.1 Reach of the LHC in various channels

Since sparticle masses are largely determined by the parameters m_0 and $m_{1/2}$ the $m_0 - M_{1/2}$

¹When more than one cut choices lead to an observable signal, we retain the choice that maximizes the quantity $S/\sqrt{S+B}$.

plane is a convenient arena for simultaneously displaying the SUSY reach of future experimental facilities together with regions already excluded by current data. Many previous reach calculations for the LHC reach are, therefore, presented in this plane (for various choices of other parameters) starting with $\tan\beta = 2$; this low of a $\tan\beta$ value is now largely excluded by the LEP2 bound on m_h . We begin our presentation with $\tan\beta = 10$, in Fig. 1. The red-shaded region on the left is excluded because either electroweak symmetry is not properly broken, or $\tilde{\tau}_1$ is the LSP, while that on the right is excluded because radiative electroweak symmetry breaking (REWSB) does not occur. The magenta region in the lower left is excluded by LEP2 bounds on $m_{\tilde{W}_1} > 103.5$ GeV, and $m_h > 114.1$ GeV (for a SM-like light Higgs h). The maximum reach is shown by the E_T^{miss} contour, where the signal events include all isolated lepton possibilities. Also shown for reference are contours of $m_{\tilde{g}} = 2$ TeV, and $m_{\tilde{q}} = 2$ TeV. The maximum reach in $m_{1/2}$ occurs for low m_0 , where squark masses are somewhat lighter than gluinos, so that $\tilde{q}\tilde{q}$, $\tilde{q}\tilde{g}$ and $\tilde{g}\tilde{g}$ production processes all have large rates. Gluinos as heavy as ~ 3 TeV may be detectable at the LHC if squarks are somewhat lighter. As m_0 increases, squark masses increase, so gluino pair production becomes the dominant sparticle production mechanism. At very large values of m_0 , the squarks (and also sleptons) essentially decouple, and the reach contours flatten out, since $m_{\tilde{g}}$ is roughly constant for each value of $m_{1/2}$. The maximal reach for 100 fb^{-1} of integrated luminosity is $m_{1/2} \sim 700$ GeV, corresponding to a gluino mass value of $m_{\tilde{g}} \sim 1800$ GeV.

The reach for SUSY signals in the individual channels introduced in the last section are shown by the various contours labelled by the corresponding topology in Fig. 1. For low values of m_0 , sleptons and squarks are relatively light, and $\tilde{g}\tilde{g}$, $\tilde{q}\tilde{q}$ and $\tilde{q}\tilde{q}$ production processes all occur at large rates; direct slepton and sneutrino pair production rates are much smaller. However, left-squarks \tilde{q}_L decay frequently into the heavier chargino and heavier neutralinos, which in turn may decay to sleptons. These cascade decays frequently terminate in isolated leptons, which together with leptons from decays from tops and stops in SUSY processes, result in large rates for leptonic signals. For a fixed value of $m_{1/2}$, as m_0 increases, \tilde{g} decay to \tilde{q}_L becomes suppressed, and $BF(\tilde{g} \rightarrow \tilde{q}_R)$ increases. Since $\tilde{q}_R \rightarrow q\tilde{Z}_1$ most of the time, cascade decays then give rise to a higher fraction of $E_T + \text{jets}$ events, and the leptonic signal from the decay of gluinos is reduced. Furthermore, since squarks become heavier relative to gluinos as m_0 is increased, the leptonic signal from directly produced \tilde{q}_L also becomes smaller. As m_0 increases even further, $\tilde{g} \rightarrow \tilde{q}_R q$ also becomes suppressed or even forbidden, and $\tilde{g} \rightarrow \tilde{t}_1 t$ (and possibly $\tilde{g} \rightarrow b\tilde{b}_{1,2}$) dominates. The decays through tops and stops gives rise again to leptonic states due to \tilde{t}_1 and t leptonic decays. This results in an increased reach at moderate m_0 values via leptonic modes such as SS and OS dileptons, and 3ℓ events. As m_0 increases even more, \tilde{g} two-body decays become completely forbidden, and three-body decays dominate, and the leptonic reach contours tend to level off.

Finally, we show a contour that marks the signal reach for events including $E_T + \text{jets}$ plus at least one isolated photon. In evaluating this reach, we have only retained physics backgrounds in our calculation. Detector-dependent backgrounds where a jet fakes

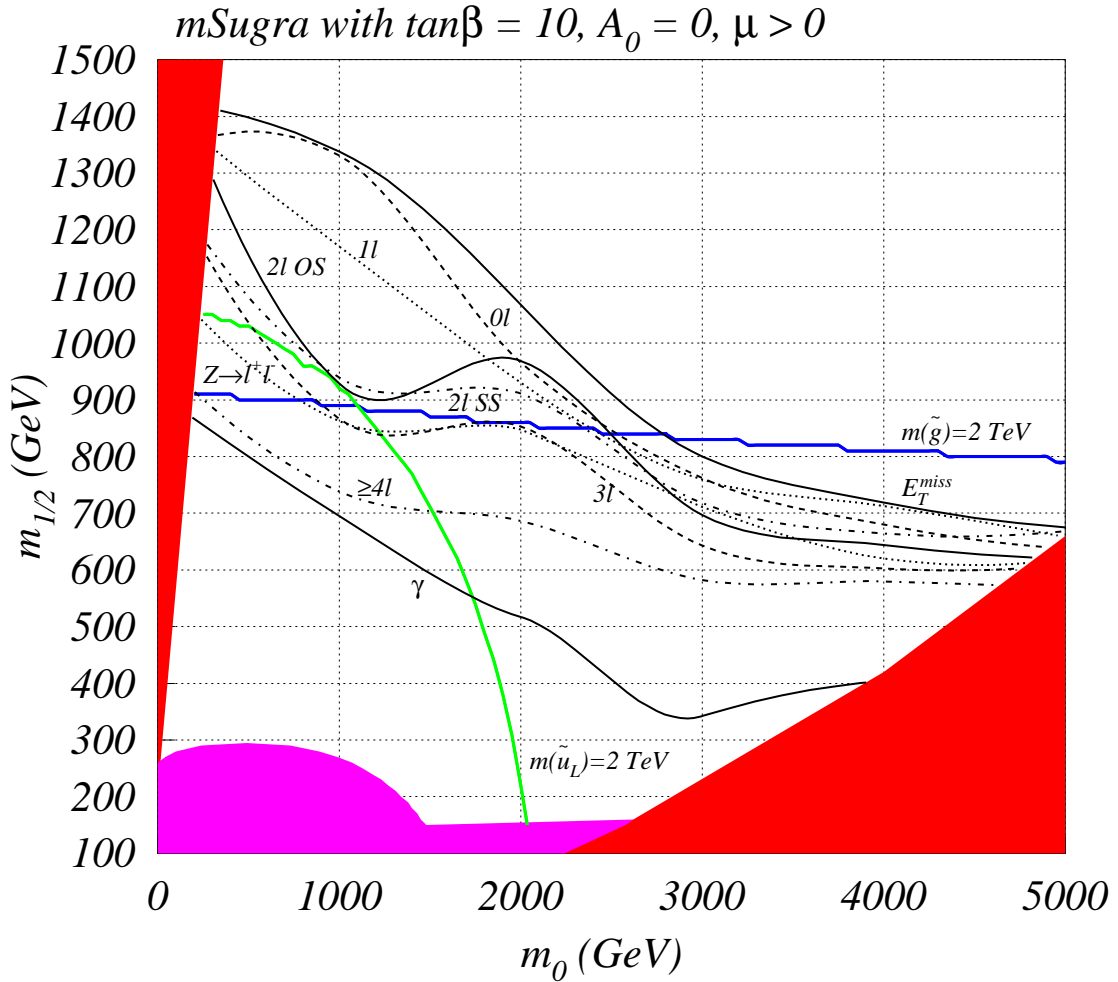


Figure 1: The reach of CERN LHC in the m_0 vs. $m_{1/2}$ parameter plane of the mSUGRA model, with $\tan\beta = 10$, $A_0 = 0$ and $\mu > 0$, assuming 100 fb^{-1} of integrated luminosity. The red (magenta) regions are excluded by theoretical (experimental) constraints discussed in the text. We show the reach in the 0ℓ , 1ℓ , OS , SS , 3ℓ , $\geq 4\ell$, γ and Z channels, as well as in the “inclusive” E_T^{miss} channel.

a photon may be significant.² In most of the parameter space, the additional photon arises from $h \rightarrow \gamma\gamma$ decay, where the h is produced copiously in sparticle cascade decays, especially from $\tilde{Z}_2 \rightarrow \tilde{Z}_1 h$. In these regions, in fact, if we require *two* isolated photons, then we can reconstruct a di-photon invariant mass. This is illustrated in Fig. 2 for the parameter space point $m_0 = m_{1/2} = 500 \text{ GeV}$, $A_0 = 0$, $\tan\beta = 30$ and $\mu > 0$. It is amusing to note that the

²If we take the probability for a jet to fake a photon to be 5×10^{-4} and assume that the hard scattering events have ~ 10 30-40 GeV “jets” in them, about one in 500 background events will also appear to have an isolated photon. Assuming that this fake photon background can be estimated by reducing the physics background in the inclusive E_T^{miss} channel by 500, we find that this background is somewhat smaller, but of the same order of magnitude as the physics background that we have evaluated. A real evaluation of this detector-dependent background is beyond the scope of our analysis.

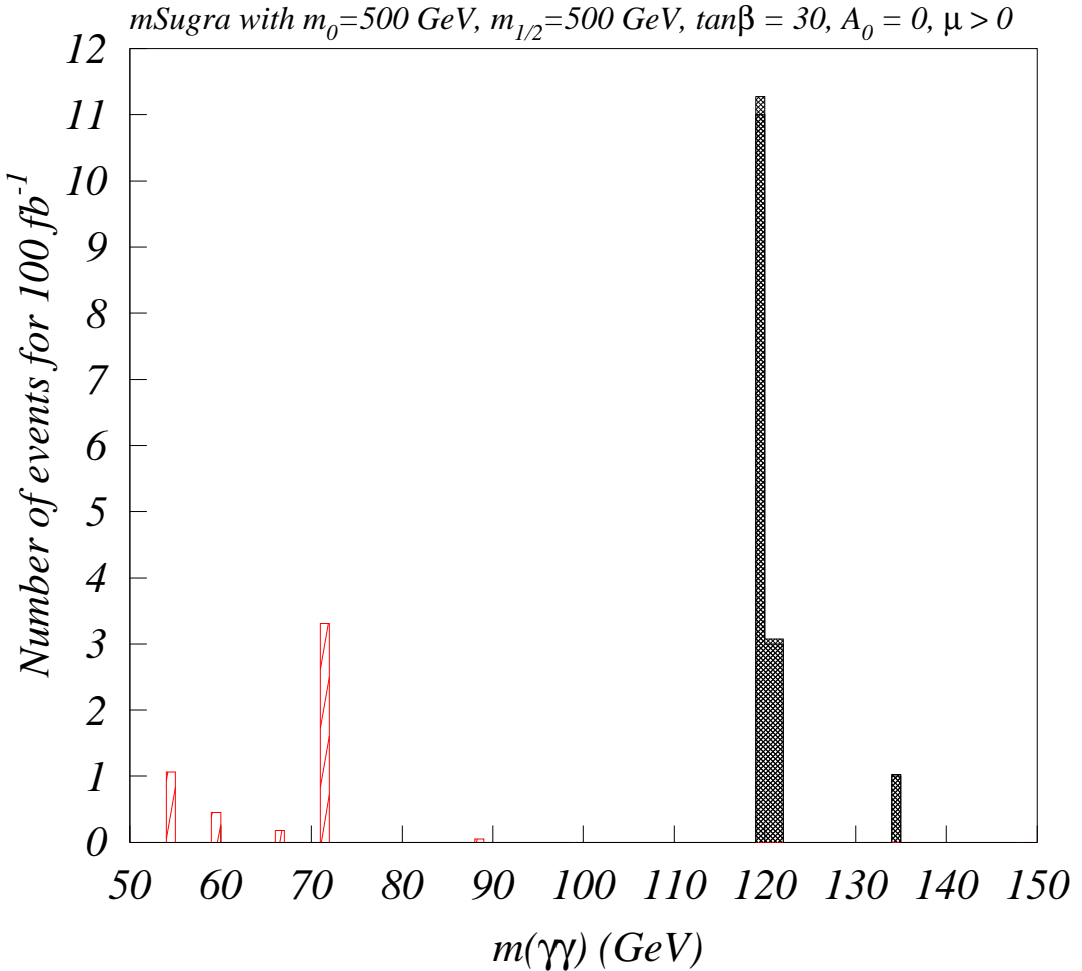


Figure 2: The diphoton invariant mass in SUSY events with two isolated photons. The shaded histogram is for diphotons from SUSY events, while the hatched histogram represents corresponding events of SM origin. The background has been obtained by scaling a Monte Carlo run for a lower value of integrated luminosity.

$h \rightarrow \gamma\gamma$ signal should be visible in SUSY events for 100 fb^{-1} of integrated luminosity. We see that (for these parameters) the highest possible luminosity is needed for the detection of this severely rate-limited, but essentially SM background-free, signal. A detection of h in this manner would nicely confirm its detection via $gg \rightarrow h \rightarrow \gamma\gamma$, where the signal would be picked out as a small peak above an enormous continuum background. A Higgs signal in the multijet plus $\gamma\gamma + E_T^{miss}$ channel would also suggest the supersymmetric origin of the Higgs production process. As m_0 becomes very large, and the region of low $|\mu|$ is approached, the radiative decay $\tilde{Z}_2 \rightarrow \tilde{Z}_1\gamma$ becomes enhanced[31]. In this HB/FP region, the isolated photon contour likewise turns up, to reflect the increase in isolated photon activity from neutralino radiative decay.

As we move to larger values of the parameter $\tan \beta$, as in Fig. 3 for $\tan \beta = 30$, the first thing to notice is that the left red-shaded region, where $\tilde{\tau}_1$ is the LSP, has expanded. This is because as $\tan \beta$ increases, both the τ (and also b) Yukawa couplings become non-negligible. This results in a reduction of stau and sbottom soft breaking masses via RGE running, and also in greater $L - R$ mixing, which again reduces the mass of the lightest eigenstates. The negative results of searches for heavy isotopes of hydrogen (or other elements) results in limits that are many orders of magnitude below their expected relic density in big-bang cosmology, so that this possibility is strongly excluded. Finally, the large values of f_b and f_τ together with the reduction of the corresponding sfermion masses relative to the first two generations mentioned above, increases various three body sparticle decays to b -quarks and τ leptons, at the expense of their first and second generation counterparts[25]. The net effect of this is to enhance sparticle cascade decays to final states containing b -quarks and τ -leptons in the low m_0 region. This results in a diminution of the reach in isolated lepton channels at low m_0 , as compared with Fig. 1. The large b and τ Yukawa couplings hardly affect the $\cancel{E}_T + jets$ and 0ℓ signals, and so the ultimate reach of the LHC changes little in proceeding from $\tan \beta = 10$ to $\tan \beta = 30$.

In Fig. 4, we show the m_0 vs. $m_{1/2}$ plane for $\tan \beta = 45$ and $\mu < 0$. The large b and τ Yukawa coupling effects are accentuated even more in this figure: a larger region is excluded at low m_0 , and the reach via multi-lepton channels is further diminished for small m_0 values where squarks and sleptons still play a role in determining cascade decay patterns. However, again, the overall reach in the $\cancel{E}_T + jets$ and 0ℓ channels is hardly affected. If we increase $\tan \beta$ much beyond about 50 for $\mu < 0$, the parameter space begins to close up fast due to a breakdown in REWSB.

In Fig. 5, we show the m_0 vs. $m_{1/2}$ plane for $\tan \beta = 52$ and $\mu > 0$. In this case, the overall reach in the $\cancel{E}_T + jets$ and 0ℓ channels is similar to the cases at lower $\tan \beta$. However, in the multi-lepton channels, there is again a suppression of reach at low m_0 . This is because for very high $\tan \beta$, $m_{\tilde{\tau}_1}$ is so light that \tilde{W}_1 dominantly decays to $\tilde{\tau}_1 \nu_\tau$ rather than $\tilde{Z}_1 W$, and likewise, $\tilde{Z}_2 \rightarrow \tilde{\tau}_1 \tau$ rather than $\tilde{Z}_1 h$ or $\tilde{Z}_1 Z$. As m_0 increases, the stau mass increases, and the $\tilde{W}_1 \rightarrow \tilde{\tau}_1 \nu_\tau$ decay mode becomes more suppressed, which increases the $\tilde{W}_1 \rightarrow \tilde{Z}_1 W$ branching fraction. The subsequent W boson decays from $\tilde{W}_1 \rightarrow \tilde{Z}_1 W$ lead to hard isolated leptons.

Our projections of the LHC reach, where they can be directly compared, are qualitatively similar to the results in Ref. [13]. Differences between the results can be attributed to the difference in the observability criteria ($S \geq 5\sqrt{S+B}$ used in Ref.[13] requires a minimum of 25 events to be compared with 10 events in our study, as well as a somewhat larger significance of the signal), and to the use of PYTHIA instead of ISAJET for event simulation.

3.2 The LHC reach in light of indirect constraints

A variety of low energy measurements have been used to obtain constraints on the parameter space of the mSUGRA model. These include the measured values of the cold dark matter density, the branching fraction $BF(b \rightarrow s\gamma)$, the value of the anomalous magnetic

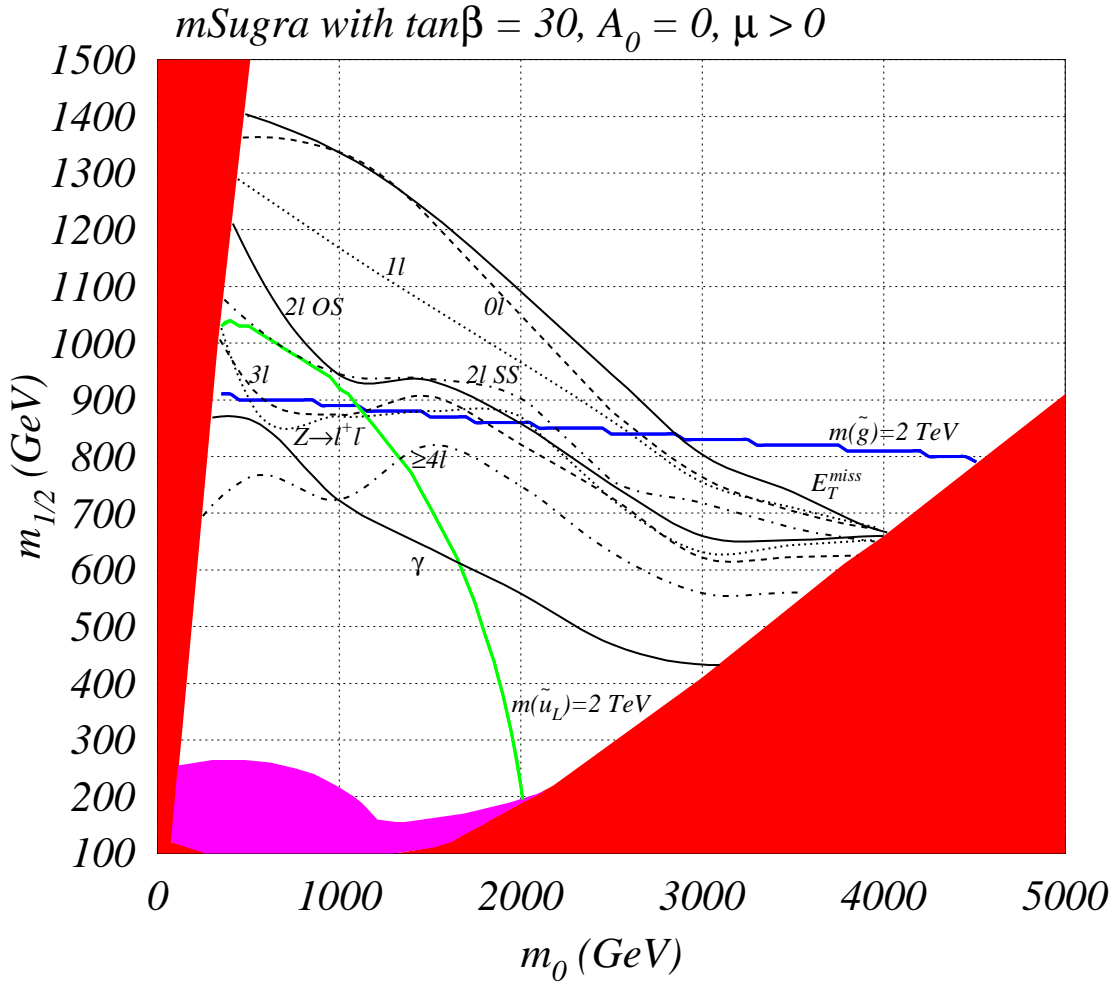


Figure 3: The reach of CERN LHC in the m_0 vs. $m_{1/2}$ parameter plane of the mSUGRA model, with $\tan\beta = 30$, $A_0 = 0$ and $\mu > 0$, assuming 100 fb^{-1} of integrated luminosity. The red (magenta) regions are excluded by theoretical (experimental) constraints discussed in the text. We show the reach in the 0ℓ , 1ℓ , OS , SS , 3ℓ , $\geq 4\ell$, γ and Z channels, as well as in the “inclusive” E_T^{miss} channel.

moment of the muon, $a_\mu = (g - 2)_\mu/2$, ³ and a lower limit on $BF(B_s \rightarrow \mu^+ \mu^-)$. Unlike collider constraints which are much more direct, constraints from the low energy measurements are considerably more sensitive to details of the model, and may be considerably altered by small modifications (which would have little impact upon collider constraints) of the underlying framework. Within a specific framework (*e.g.* mSUGRA), however, these indirect constraints exclude certain regions of parameter space, and also suggest other regions where future searches might be focussed.

Neutralino relic density:

³There is considerable theoretical uncertainty in the SM value of a_μ , so that caution must be exercised in interpreting the result of experiment E821.

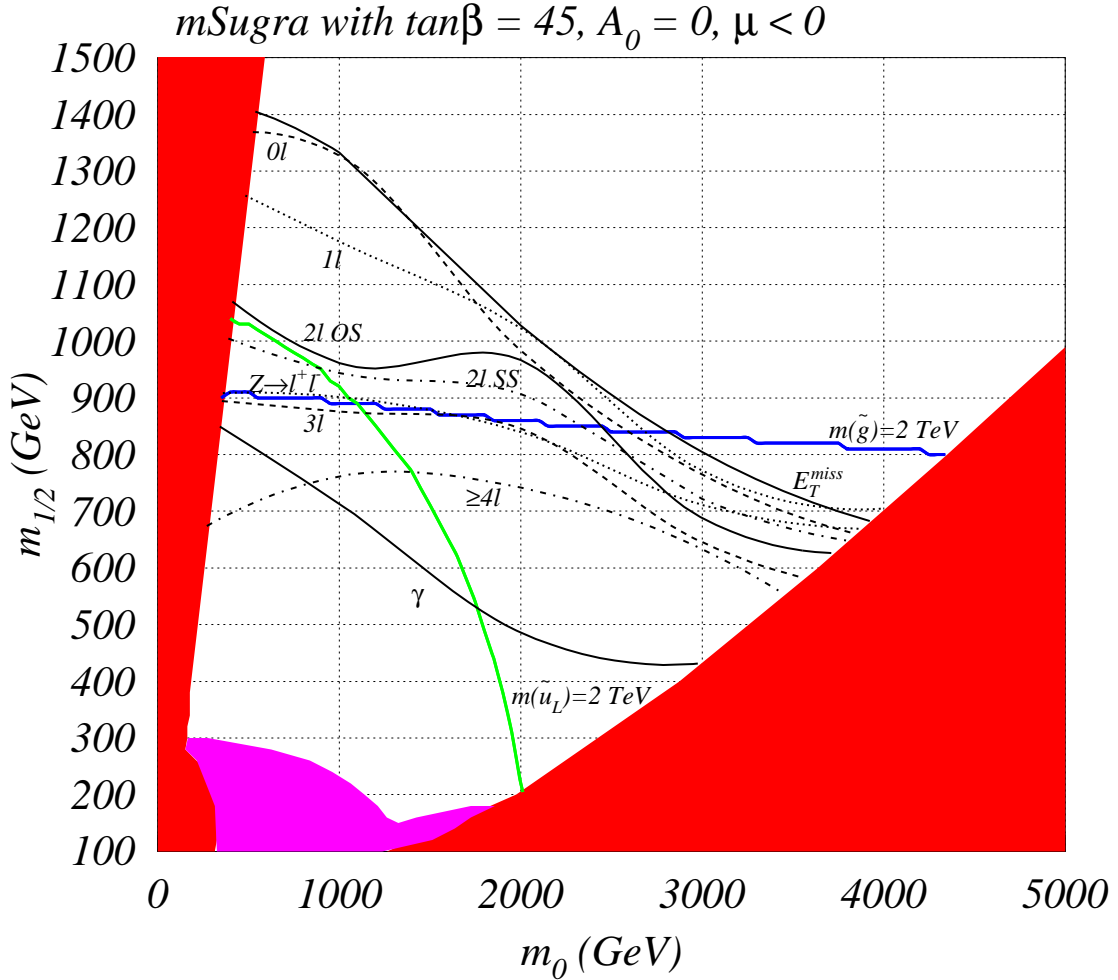


Figure 4: The reach of CERN LHC in the m_0 vs. $m_{1/2}$ parameter plane of the mSUGRA model, with $\tan\beta = 45$, $A_0 = 0$ and $\mu < 0$, assuming 100 fb^{-1} of integrated luminosity. The red (magenta) regions are excluded by theoretical (experimental) constraints discussed in the text. We show the reach in the 0ℓ , 1ℓ , OS , SS , 3ℓ , $\geq 4\ell$, γ and Z channels, as well as in the “inclusive” E_T^{miss} channel.

Measurements of galactic rotation curves, binding of galactic clusters, and the large scale structure of the universe all point to the need for significant amounts of cold dark matter (CDM) in the universe. In addition, recent measurements of the power spectrum of the cosmic microwave background from WMAP and other data sets[3] lead to

- $\Omega_{CDM}h^2 = 0.1126^{+0.008}_{-0.009}$.

The upper limit derived from this is a true constraint on any stable relic from the Big Bang, such as the lightest neutralino of the mSUGRA model. Regions of mSUGRA parameter space which result in a relic density that violates this bound are excluded. A remarkable feature of the model is that there are regions of the parameter space where the neutralino density lies in the observed range, so that the neutralino makes up almost all the cold dark matter in the universe. We remark, however, that unlike the upper limit above, the

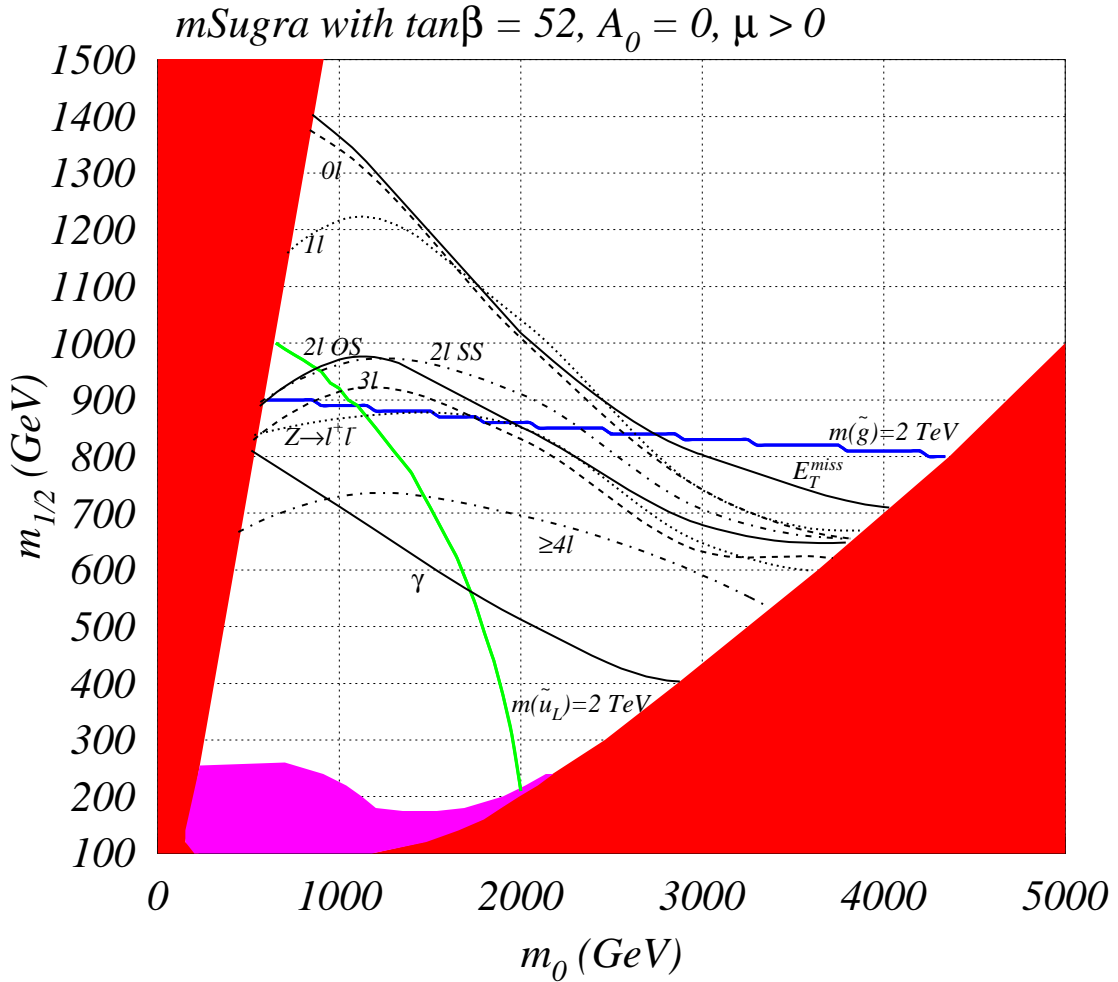


Figure 5: The reach of CERN LHC in the m_0 vs. $m_{1/2}$ parameter plane of the mSUGRA model, with $\tan\beta = 52$, $A_0 = 0$ and $\mu > 0$, assuming 100 fb^{-1} of integrated luminosity. The red (magenta) regions are excluded by theoretical (experimental) constraints discussed in the text. We show the reach in the 0ℓ , 1ℓ , OS , SS , 3ℓ , $\geq 4\ell$, γ and Z channels, as well as in the “inclusive” E_T^{miss} channel.

corresponding lower limit is flexible, since there may be additional sources of CDM such as axions, or states associated with the hidden sector of the mSUGRA model and/or extra dimensions.

To estimate the relic density of neutralinos in the mSUGRA model, we use the recent calculation in Ref. [35]. All relevant neutralino annihilation and co-annihilation reactions are included along with relativistic thermal averaging[36], which is important for obtaining the correct neutralino relic density in the vicinity of annihilations through s -channel resonances.

BF($b \rightarrow s\gamma$):

The branching fraction $BF(b \rightarrow s\gamma)$ has recently been measured by the BELLE[37],

CLEO[38] and ALEPH[39] collaborations. Combining statistical and systematic errors in quadrature, these measurements give $(3.36 \pm 0.67) \times 10^{-4}$ (BELLE), $(3.21 \pm 0.51) \times 10^{-4}$ (CLEO) and $(3.11 \pm 1.07) \times 10^{-4}$ (ALEPH). A weighted averaging of these results yields $BF(b \rightarrow s\gamma) = (3.25 \pm 0.37) \times 10^{-4}$. The 95% CL range corresponds to $\pm 2\sigma$ away from the mean. To this we should add uncertainty in the theoretical evaluation, which within the SM dominantly comes from the scale uncertainty, and is about 10%. Together, these imply the bounds,

- $2.16 \times 10^{-4} < BF(b \rightarrow s\gamma) < 4.34 \times 10^{-4}$.

The evaluation of the SUSY contribution to this decay entails additional theoretical uncertainties, especially when $\tan\beta$ is large, so that this range should be relaxed somewhat. In our study, we show contours of $BF(b \rightarrow s\gamma)$ of 2, 3, 4 and 5×10^{-4} .

The calculation of $BF(b \rightarrow s\gamma)$ used here is based upon the program of Ref. [40]. In our calculations, we also implement the running b -quark mass including SUSY threshold corrections as calculated in ISAJET; these effects can be important at large values of the parameter $\tan\beta$ [41]. Our value of the SM $b \rightarrow s\gamma$ branching fraction yields 3.4×10^{-4} , with a scale uncertainty of 10%.

Muon anomalous magnetic moment

The muon anomalous magnetic moment $a_\mu = (g - 2)_\mu/2$ has been recently measured to high precision by the E821 experiment[42]: $a_\mu = 11659204(7)(5) \times 10^{-10}$. The most challenging parts of the SM calculation are the hadronic light-by-light[43] and vacuum polarization (HVP)[44] contributions and their uncertainties. Presently these results are in dispute. In the case of the HVP the use of tau decay data can reduce the error, but the interpretation of these data is somewhat controversial[45]. Thus, the deviation of the measurement from the SM depends on which prediction is taken into account. According to the recent analysis by Hagiwara et al.[44]:

- $11.5 < \delta a_\mu \times 10^{10} < 60.7$.

A different assessment of the theoretical uncertainties[44] using the procedure described in Ref.[46] gives,

- $-16.7 < \delta a_\mu \times 10^{10} < 49.1$.

Yet another determination has recently been made by Narison, includes additional scalar meson loops[47]. This, using $e^+e^- \rightarrow \text{hadrons}$ data to evaluate hadronic vacuum polarization contributions, yields

- $-3.9 < \delta a_\mu \times 10^{10} < 52.1$,

while using τ -decay data results in

- $-26.7 < \delta a_\mu \times 10^{10} < 30.1$.

The latter may include additional systematic uncertainties from how isospin breaking effects are incorporated.

In view of the theoretical uncertainty, we only present contours of δa_μ , as calculated using the program developed in [48], and leave it to the reader to decide the extent of the parameter region allowed by the data.

$B_s \rightarrow \mu^+\mu^-$ decay

The branching fraction of B_s to a pair of muons has been experimentally bounded by CDF[49]:

- $BF(B_s \rightarrow \mu^+ \mu^-) < 2.6 \times 10^{-6}$.

If $\tan \beta \lesssim 20 - 25$ SUSY contributions to this decay are small and do not lead to new constraints on the parameter space. If $\tan \beta$ is large, the important SUSY contribution to this decay is mediated by the neutral states in the Higgs sector of supersymmetric models. While this branching fraction is very small within the SM ($BF_{SM}(B_s \rightarrow \mu^+ \mu^-) \simeq 3.4 \times 10^{-9}$), the amplitude for the Higgs-mediated decay of B_s roughly grows as $\tan^3 \beta$,⁴ and hence can completely dominate the SM contribution if $\tan \beta$ is large. In our analysis we use the results from the last paper in Ref. [50] to delineate the region of mSUGRA parameters excluded by the CDF upper limit on its branching fraction.

In Fig. 6, we again show the m_0 vs. $m_{1/2}$ plot for $\tan \beta = 10$, $A_0 = 0$ and $\mu > 0$. This time, we exhibit contours for the low energy observables mentioned above, as mapped out in Ref. [46]. A χ^2 analysis of the indirect constraints was performed in Ref. [51], which helped to identify regions of parameter space allowed by all the combined indirect constraints. Several regions emerge in the m_0 vs. $m_{1/2}$ plane where the relic density can be within the WMAP range. At low m_0 and low $m_{1/2}$, neutralino annihilation through t -channel sleptons can occur with a high rate. Much of this so-called “bulk” region is largely excluded by the LEP2 Higgs bound (shown as the red contour), and in addition, $BF(b \rightarrow s\gamma)$, though in the acceptable range, is below its experimental central value. In this region, sparticles are very light, and a SUSY discovery by the CERN LHC should be easy.

One of the remaining regions allowed by relic density constraint is the very narrow strip adjacent to the “ \tilde{Z}_1 not LSP” region at low m_0 , where stau co-annihilation is important[52]. We see that the reach of the LHC apparently covers much of the stau co-annihilation strip, up to $m_{1/2} \sim 1400$ GeV for 100 fb^{-1} of integrated luminosity. To determine the LHC reach needed to completely explore the stau co-annihilation strip, we show the relic density for fixed $m_{1/2}$ values vs. m_0 in Fig. 7. In frame *a*), it is evident that an LHC reach up to $m_{1/2} \sim 1700$ GeV (for $m_0 \lesssim 450$ GeV) would completely explore this co-annihilation corridor for $\tan \beta = 10$.

The other region allowed by relic density constraint occurs at very large m_0 where μ becomes small: the HB/FP region[32, 33].⁵ Here, the growing higgsino component of the neutralino allows for efficient annihilation into vector boson pairs[53, 55]. For very small μ values, then neutralino-chargino co-annihilation becomes important[56]. In this FP/HB region squarks are very heavy, and as $m_{1/2}$ increases, $m_{\tilde{g}}$ increases as well so that strongly interacting sparticle production cross sections decrease. Since μ is small, the light charginos and neutralinos are significantly higgsino-like, and can only be produced via electroweak interactions. We see that the reach of the LHC is limited to $m_{1/2} \sim 700$ GeV. For even higher $m_{1/2}$ values, and staying in the HB/FP region, one enters an area that is not be accessible to LHC experiments, at least via the general purpose search strategies described here, even though the light charginos and neutralinos are expected to have masses less

⁴The $\tan^3 \beta$ growth obtains if the tree-level value of m_b is fixed. For large values of $\tan \beta$, the radiative correction to m_b is important resulting in a deviation from the $\tan^3 \beta$ growth.

⁵The entire HB/FP region is not shown here: over part of this region, the evaluation of the μ parameter using Isajet 7.64 is numerically unstable. This is corrected in ISAJET v7.65.

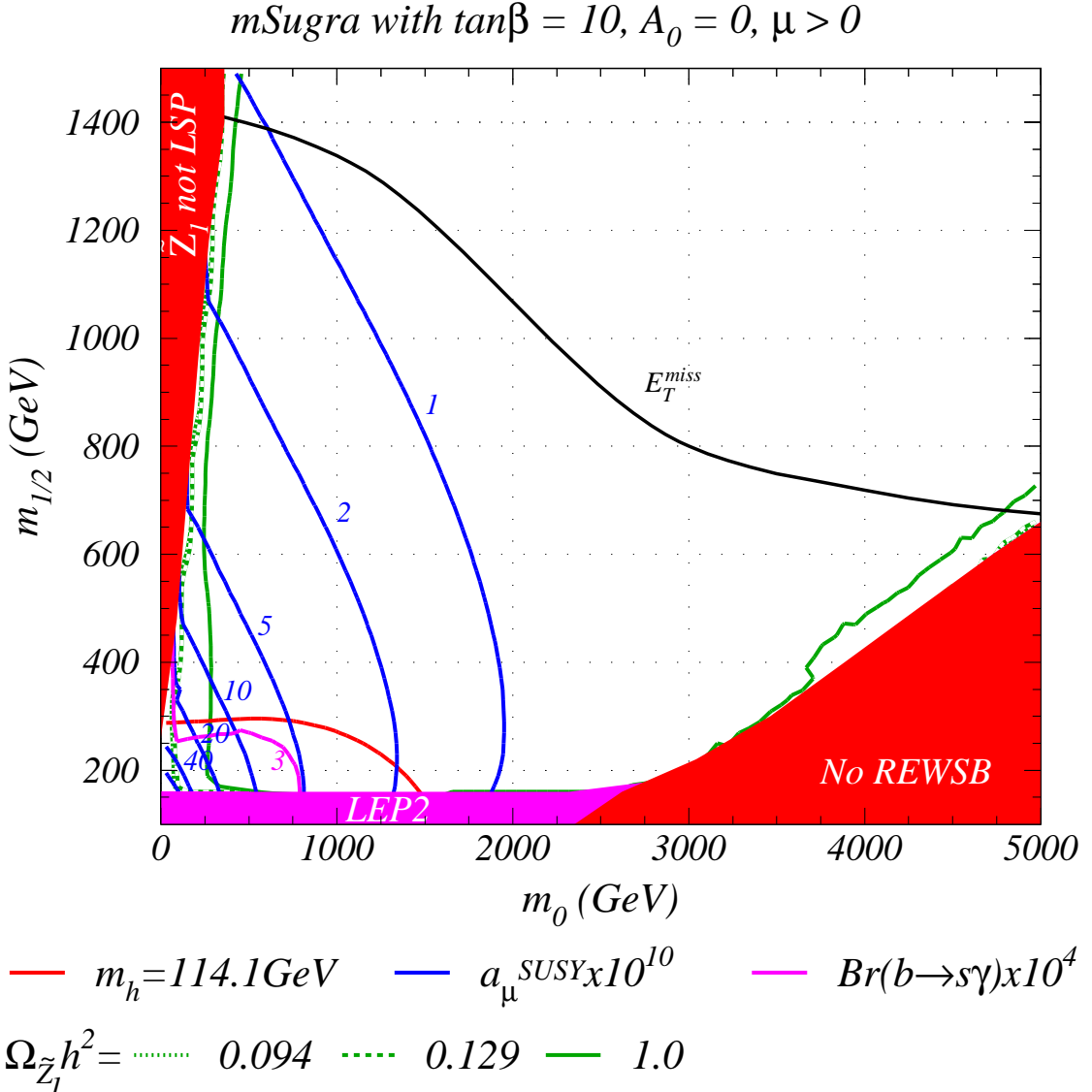


Figure 6: Contours of several low energy observables in the m_0 vs. $m_{1/2}$ plane of the mSUGRA model, for $\tan\beta = 10$, $A_0 = 0$ and $\mu > 0$. We show contours of CDM relic density (green), together with a contour of $m_h = 114.1$ GeV (red), contours of muon anomalous magnetic moment a_μ ($\times 10^{10}$) (blue) and contours of $b \rightarrow s\gamma$ branching fraction ($\times 10^4$) (magenta). Also shown is the maximal reach of the CERN LHC in the $\cancel{E}_T + \text{jets}$ channel for 100 fb^{-1} of integrated luminosity.

than 250-500 GeV. It would be interesting to examine whether it is possible to devise search strategies that exploit specific characteristics of the FP/HB region to extend the LHC reach. For instance, in the small $|\mu|$ region, decays of gluinos into third generation fermions are enhanced resulting in events with hard b and t quarks from the decay of heavy gluinos. Whether it is possible to extend the LHC reach in these event topologies merits further investigation.

Next, we show the contours for the same low energy observables as in Fig. 6, but for

mSUGRA

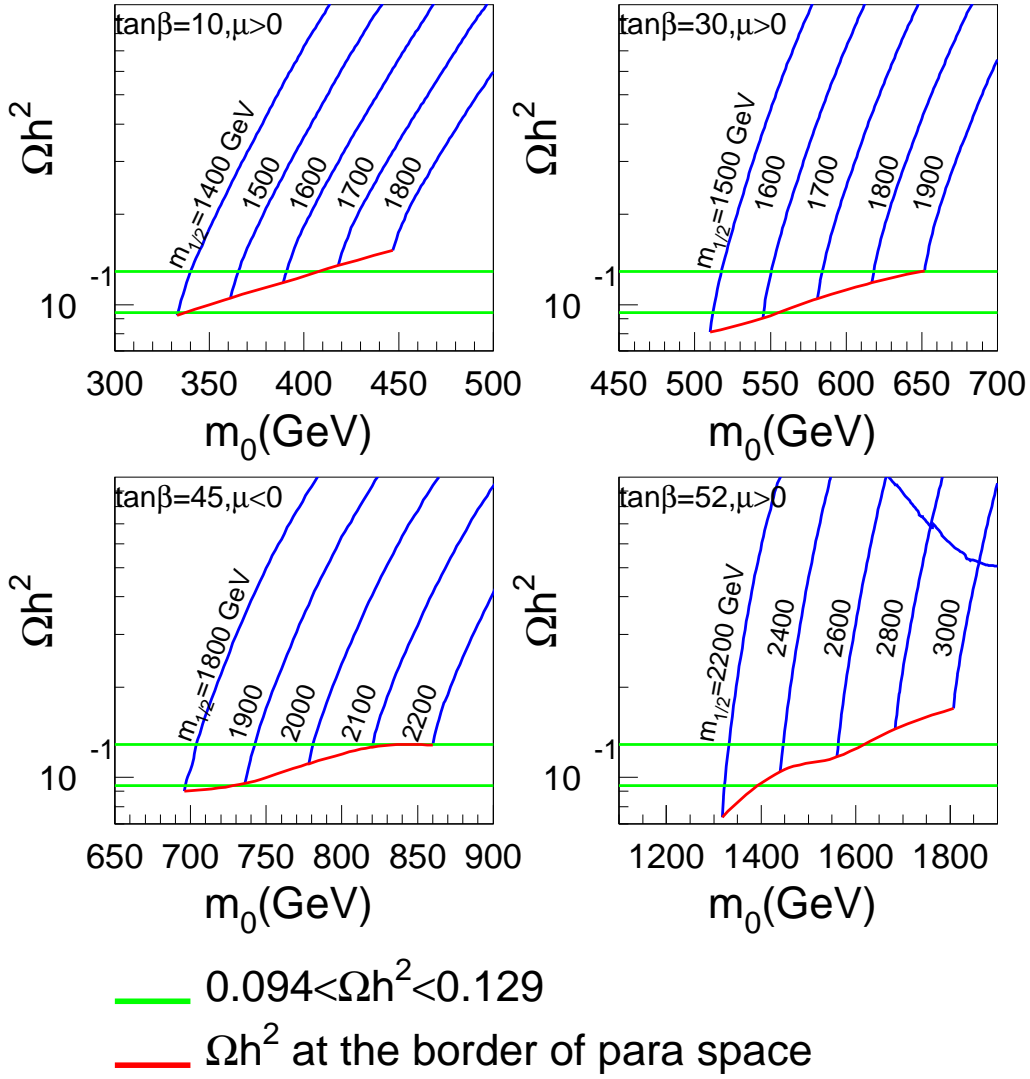


Figure 7: The relic density $\Omega_{\tilde{Z}_1} h^2$ vs. m_0 for various fixed $m_{1/2}$ values in the stau co-annihilation corridor, for a) $\tan \beta = 10, \mu > 0$, b) $\tan \beta = 30, \mu > 0$, c) $\tan \beta = 45, \mu < 0$ and $\tan \beta = 52, \mu > 0$. We also show via green lines the 2σ WMAP limits on $\Omega_{\tilde{Z}_1} h^2$.

$\tan \beta = 30$, $A_0 = 0$ and $\mu > 0$ in Fig. 8. The larger value of $\tan \beta$ causes the values a_μ and $BF(b \rightarrow s\gamma)$ to deviate more from their SM values at low m_0 and $m_{1/2}$; the bulk region of relic density annihilation is disfavored by $BF(b \rightarrow s\gamma)$. This leaves only the stau co-annihilation corridor and the HB/FP region as phenomenologically viable. The LHC reach contour remains similar to that for $\tan \beta = 10$. Again, we see that if SUSY has

mSugra with $\tan\beta = 30, A_0 = 0, \mu > 0$

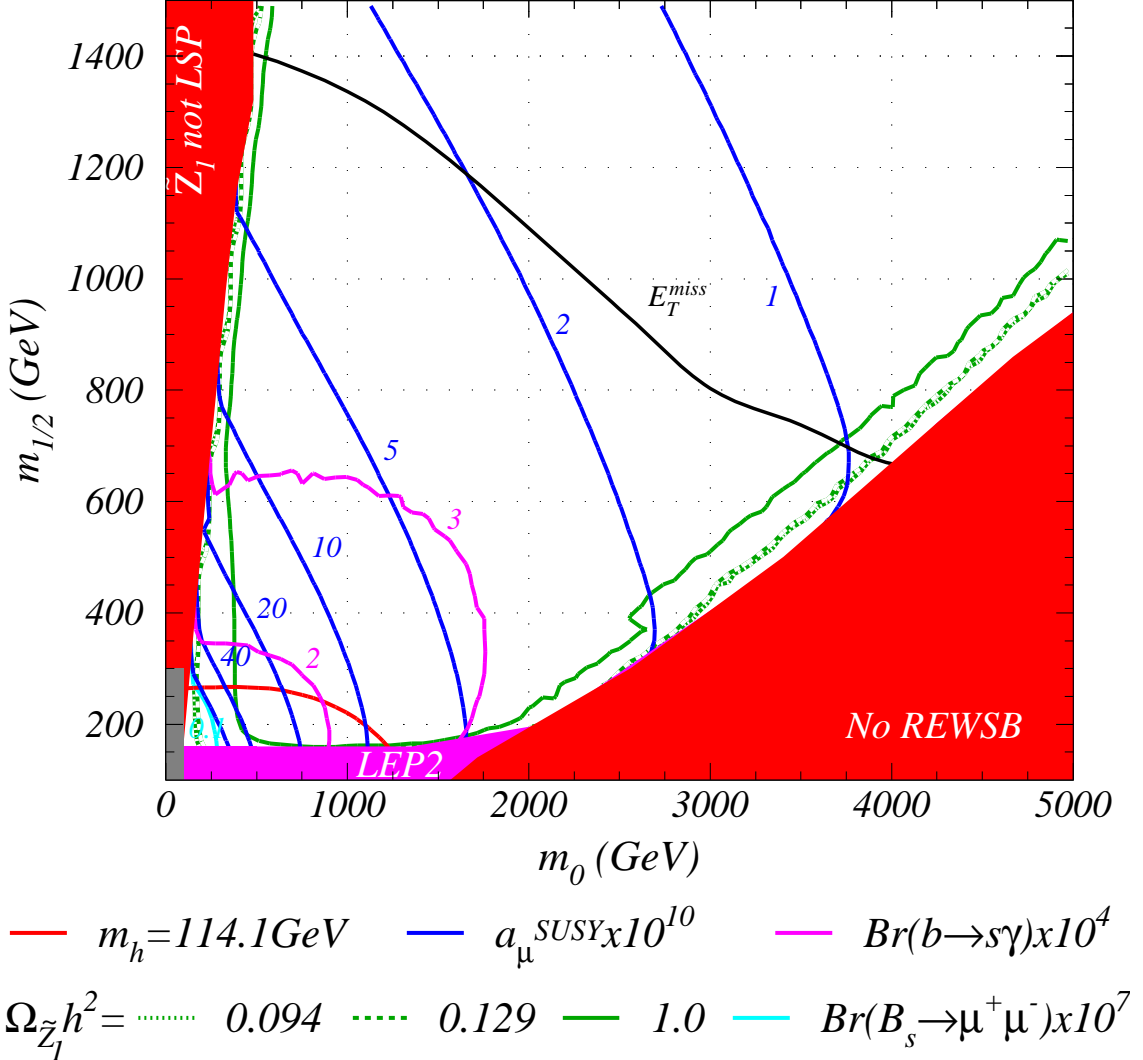


Figure 8: The same as Fig. 6 but for $\tan\beta = 30$.

parameters in this plane, then LHC should see it unless *i.*) $1400 \text{ GeV} < m_{1/2} < 1900 \text{ GeV}$ with m_0 in the stau co-annihilation strip, as depicted in Fig. 7b, or *ii.*) $m_{1/2} > 700 \text{ GeV}$ with SUSY in the HB/FP region.

Fig. 9 illustrates the impact of the low energy observables, this time for $\tan\beta = 45$ and $\mu < 0$. The LHC reach is similar to the lower $\tan\beta$ cases, but now the low m_0 and $m_{1/2}$ bulk region is firmly excluded by both a_μ and $BF(b \rightarrow s\gamma)$, which are large negative, and large positive, respectively. We see, however, that a new region of low relic density has opened up: the $\tilde{Z}_1 \tilde{Z}_1 \rightarrow A$, $H \rightarrow f\bar{f}$ annihilation corridor, where annihilation takes place especially through the very broad A width[53, 54]. In fact, we see that although the A annihilation corridor extends to very large $m_{1/2}$ values, the region allowed by WMAP

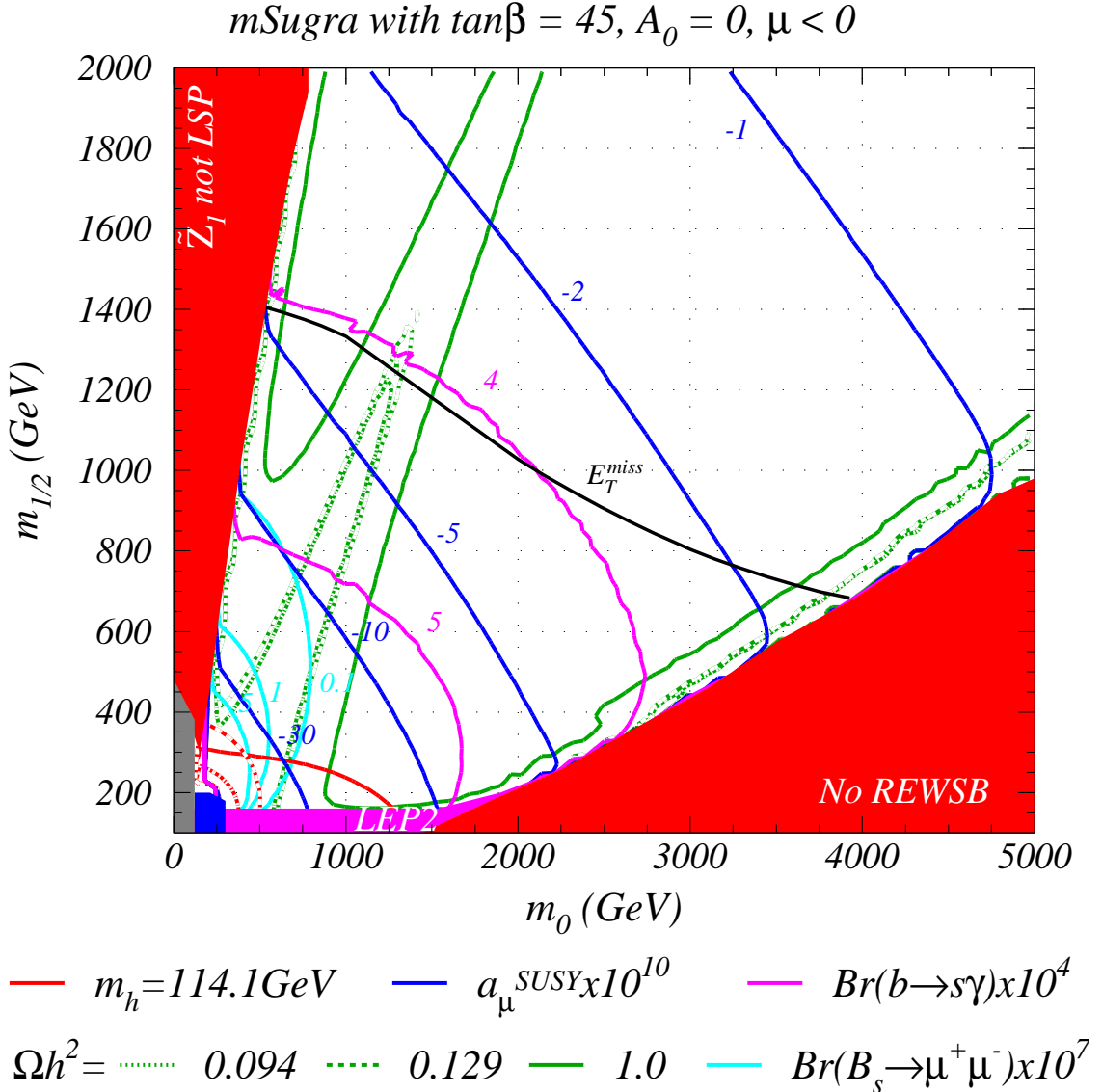


Figure 9: The same as Fig. 6 but for $\tan\beta = 45$ and $\mu < 0$.

is almost entirely accessible to LHC searches. A modest additional integrated luminosity beyond 100 fb^{-1} assumed in this study should cover this entire region. In addition, the stau co-annihilation corridor remains consistent with WMAP constraints up to $m_{1/2}$ values as high as 2200 GeV as shown in frame *c*) of Fig. 7, which corresponds to $m_{\tilde{g}} \sim 4500$ GeV, well beyond the LHC reach. Finally, the HB/FP region can again be explored up to $m_{1/2} \sim 700$ GeV at the LHC.

In Fig. 10, we show the same low energy contours in the m_0 vs. $m_{1/2}$ plane, but now for $\tan\beta = 52$ and $\mu > 0$. In this case, the low m_0 and $m_{1/2}$ bulk region is largely excluded because $BF(b \rightarrow s\gamma) < 2 \times 10^{-4}$. The WMAP constraints again restrict us to either the stau co-annihilation region at low m_0 , or the HB/FP region at large m_0 . We

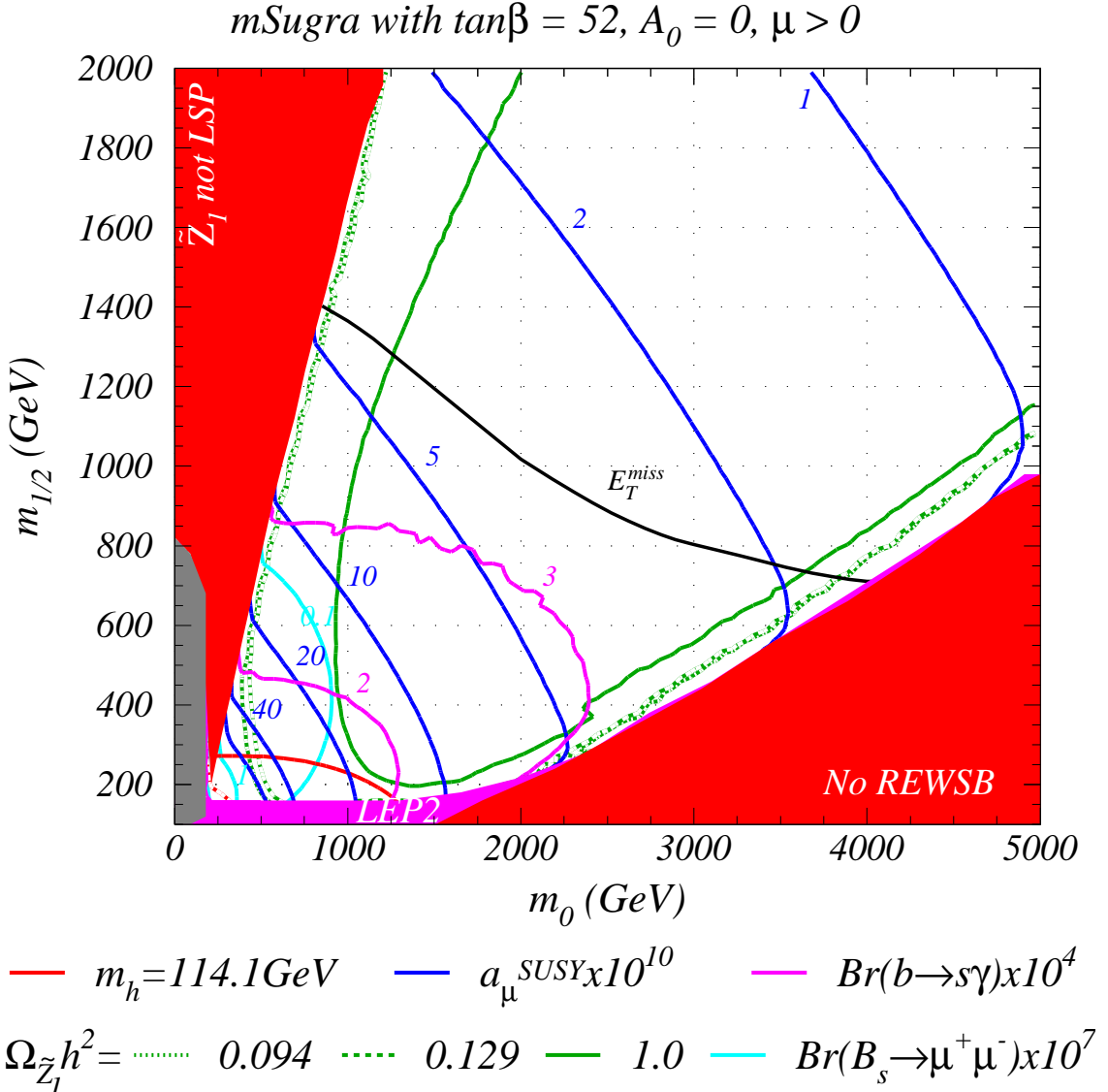


Figure 10: The same as Fig. 6 but for $\tan\beta = 45$.

can see from Fig. 7d that the stau co-annihilation corridor extends to $m_{1/2} \sim 2700$ GeV, which is well beyond the reach of the LHC. Models with these high parameter values suffer from considerable fine-tuning, since the μ parameter, which has been invoked as a measure of fine-tuning[32], is beyond 1600 GeV for $m_{1/2} > 1400$ GeV, so that μ^2/M_Z^2 is large. In the HB/FP region, the LHC reach, via these channels, again cuts off at $m_{1/2} \sim 700$ GeV: once again, it would be worth exploring whether the SUSY signal can be picked up in other channels.

4. Conclusions

We have updated our assessment of the SUSY reach of the CERN LHC via E_T^{miss} and multilepton channels, and presented new results for the reach in channels with isolated photons or leptonically decaying Z bosons. We work within the framework of the mSUGRA model, and use ISAJET v7.64 together with the CMSJET fast detector simulation to model the CMS detector, and assume an integrated luminosity of 100 fb^{-1} . Our results are presented over an expanded mSUGRA model parameter space to include the reach in the so-called HB/FP region at very large m_0 . This region, together with the stau coannihilation corridor, and the annihilation funnel where LSPs annihilate via the A or H resonances, are strongly preferred by the recent data of the WMAP collaboration. The overall LHC reach turns out to be quite insensitive to $\tan \beta$. We find that experiments at the LHC will probe $m_{1/2} \lesssim 1400 \text{ GeV}$ for low m_0 , and $m_{1/2} \sim 700$ for large m_0 in the HB/FP region. These values correspond to $m_{\tilde{g}} \sim 3000 \text{ GeV}$ and 1800 GeV , respectively.

We have also presented the reach in a variety of multi-lepton channels. The reach in these individual channels is, in general, sensitive to $\tan \beta$. We also show the reach in a channel including reconstructed $Z^0 \rightarrow \ell\bar{\ell}$ decays, and channels including isolated photons. The isolated photon signals may contain $h \rightarrow \gamma\gamma$ events at a low, but observable rate. Indeed the SUSY event sample may contain SM background-free $h \rightarrow \gamma\gamma$ events, though a very high integrated luminosity will be needed to identify the rate-limited h signal. In the HB/FP region, the photonic channels also have a slight enhancement from radiative neutralino decays $\tilde{Z}_2 \rightarrow \tilde{Z}_1\gamma$. For $m_{1/2} \lesssim 800(400) \text{ GeV}$ and small (large) values of m_0 , there should be observable signals in all these channels if new physics discovered at the LHC is to be interpreted as supersymmetry as realized in the mSUGRA model.

We have also examined the reach of the LHC in light of the recent assessment of direct (from LEP2) and indirect constraints on the mSUGRA model. The indirect constraints include the neutralino relic density $\Omega_{\tilde{Z}_1} h^2$ from recent WMAP analyses together with accelerator measurements of $BF(b \rightarrow s\gamma)$, $a_\mu = (g-2)_\mu$ and the bound on $BF(B_s \rightarrow \mu^+\mu^-)$ (this bound is hardly constraining for the parameter planes that we have examined). For large values of $\tan \beta$, experimental values of $BF(b \rightarrow s\gamma)$ and a_μ disfavor negative values of the μ parameter unless m_0 and $m_{1/2}$ are also large, but for $\tan \beta \sim 10$, values of m_0 and $m_{1/2} \gtrsim 400 - 500 \text{ GeV}$ are perfectly acceptable. For $\mu > 0$, m_0 would have to be rather small so that the relic density is either in the bulk annihilation region or in the stau coannihilation strip, or m_0 would have to be very large, in the HB/FP region. The CERN LHC can definitely explore all the bulk annihilation region, and can explore all the stau coannihilation corridor for low $\tan \beta$, but not for high $\tan \beta$. The LHC can explore the HB/FP region up to $m_{1/2} \sim 700 \text{ GeV}$ via the conventional SUSY search channels. However, the HB/FP region appears to extend indefinitely to large $m_{1/2}$ and m_0 values, ultimately well beyond the LHC reach.

Acknowledgments

This research was supported in part by the U.S. Department of Energy under contracts

number DE-FG02-97ER41022 and DE-FG03-94ER40833.

References

- [1] For recent reviews, see *e.g.* S. Martin, in *Perspectives on Supersymmetry*, edited by G. Kane (World Scientific), [hep-ph/9709356](#); M. Drees, [hep-ph/9611409](#); J. Bagger, [hep-ph/9604232](#); X. Tata, *Proc. IX J. Swieca Summer School*, J. Barata, A. Malbouisson and S. Novaes, Eds., [hep-ph/9706307](#); S. Dawson, Proc. TASI 97, J. Bagger, Ed., [hep-ph/9712464](#).
- [2] H. Baer, C. Balázs, A. Belyaev, J. K. Mizukoshi, X. Tata and Y. Wang, *J. High Energy Phys.* **0207** (2002) 050 and [hep-ph/0210441](#); for a review, see G. Eigen, R. Gaitskell, G. Kribs and K. Matchev, [hep-ph/0112312](#).
- [3] C. L. Bennett *et al.*, Preliminary Maps and Basic Results,” [arXiv:astro-ph/0302207](#); D. N. Spergel *et al.*, Determination of Cosmological Parameters,” [arXiv:astro-ph/0302209](#).
- [4] For a recent review, see K. Olive, [arXiv:astro-ph/0301505](#) (2003).
- [5] Joint HEP2 Supersymmetry Working Group, *Combined Chargino Results, up to 208 GeV*, http://alephwww.cern.ch/lepsusy/www/inos_moriond01/charginos.pub.html.
- [6] LEP Higgs Working Group Collaboration, [hep-ex/0107030](#).
- [7] A. Chamseddine, R. Arnowitt and P. Nath, *Phys. Rev. Lett.* **49** (1982) 970; R. Barbieri, S. Ferrara and C. Savoy, *Phys. Lett.* **B 119** (1982) 343; L. J. Hall, J. Lykken and S. Weinberg, *Phys. Rev.* **D 27** (1983) 2359; for a review, see H. P. Nilles, *Phys. Rept.* **110** (1984) 1.
- [8] H. Baer, C. H. Chen, C. Kao and X. Tata, *Phys. Rev.* **D 52** (1995) 1565; H. Baer, C. H. Chen, F. Paige and X. Tata, *Phys. Rev.* **D 54** (1996) 5866; H. Baer, C. H. Chen, M. Drees, F. Paige and X. Tata, *Phys. Rev.* **D 58** (1998) 075008.
- [9] H. Baer, M. Drees, F. Paige, P. Quintana and X. Tata, *Phys. Rev.* **D 61** (2000) 095007.
- [10] V. Barger and C. Kao, *Phys. Rev.* **D 60** (1999) 115015.
- [11] K. Matchev and D. Pierce, *Phys. Rev.* **D 60** (1999) 075004 and *Phys. Lett.* **B 467** (1999) 225
- [12] H. Baer, C. H. Chen, F. Paige and X. Tata, *Phys. Rev.* **D 52** (1995) 2746 and *Phys. Rev.* **D 53** (1996) 6241.
- [13] S. Abdullin and F. Charles, *Nucl. Phys.* **B 547** (1999) 60.
- [14] S. Abdullin *et al.* (CMS Collaboration), [hep-ph/9806366](#).
- [15] ATLAS Collaboration, “ATLAS Physics and Detector Performance Technical Design Report”, LHCC 99-14/15.
- [16] H. Baer, C. H. Chen, M. Drees, F. Paige and X. Tata, *Phys. Rev.* **D 59** (1999) 055014.
- [17] H. Baer, C. H. Chen, F. Paige and X. Tata, *Phys. Rev.* **D 49** (1994) 3283; D. Denegri, W. Majerotto and L. Rurua, *Phys. Rev.* **D 58** (1998) 095010 and *Phys. Rev.* **D 60** (1999) 035008.
- [18] H. Baer, C. H. Chen, F. Paige and X. Tata, *Phys. Rev.* **D 50** (1994) 4508.
- [19] H. Baer, C. H. Chen and X. Tata, *Phys. Rev.* **D 55** (1997) 1466.
- [20] S. Bityukov and N. Krasnikov, *Phys. Lett.* **B 469** (1999) 149 and [hep-ph/0102179](#).

- [21] H. Baer, A. Belyaev, T. Krupovnickas and X. Tata, *Phys. Rev. D* **65** (2002) 075024.
- [22] H. Baer, P. Mercadante, F. Paige, X. Tata and Y. Wang, *Phys. Lett. B* **435** (1998) 109; H. Baer, P. Mercadante, X. Tata and Y. Wang, *Phys. Rev. D* **62** (2000) 095007.
- [23] H. Baer, J. K. Mizukoshi and X. Tata, *Phys. Lett. B* **488** (2000) 367; A. Barr, C. Lester, M. Parker, A. Allanach and P. Richardson, *J. High Energy Phys.* **0303** (2003) 045.
- [24] H. Baer, J. Ellis, G. Gelmini, D. Nanopoulos and X. Tata, *Phys. Lett. B* **161** (1985) 175; G. Gamberini, *Z. Physik C* **30** (1986) 605; H. Baer, V. Barger, D. Karatas and X. Tata, *Phys. Rev. D* **36** (1987) 96; R. M. Barnett, J. F. Gunion and H. Haber, *Phys. Rev. D* **37** (1988) 1892; H. Baer, X. Tata and J. Woodside, *Phys. Rev. D* **42** (1990) 1568; A. Bartl, W. Majerotto, B. Mösslacher, N. Oshimo and S. Stippel, *Phys. Rev. D* **43** (1991) 2214; H. Baer, M. Bisset, X. Tata and J. Woodside, *Phys. Rev. D* **46** (1992) 303. A. Bartl, W. Majerotto and W. Porod, *Z. Physik C* **64** (1994) 499; A. Djouadi and Y. Mambrini and M. Muhlleitner, *Eur. Phys. J. C* **20** (2001) 563; J. Hisano, K. Kawagoe and M. Nojiri, [hep-ph/0304214](#).
- [25] H. Baer, C. H. Chen, M. Drees, F. Paige and X. Tata, *Phys. Rev. Lett.* **79** (1997) 986.
- [26] H. Baer, F. Paige, S. Protopopescu and X. Tata, [hep-ph/0001086](#).
- [27] B. Allanach, S. Kraml and W. Porod, [hep-ph/0302102](#).
- [28] M. Nojiri and Y. Yamada, *Phys. Rev. D* **60** (1999) 015006;
- [29] H. Baer, X. Tata and J. Woodside, *Phys. Rev. D* **42** (1990) 1450.
- [30] H. Haber and D. Wyler, *Nucl. Phys. B* **323** (1989) 267; S. Ambrosanio and B. Mele, *Phys. Rev. D* **55** (1997) 1399.
- [31] H. Baer and T. Krupovnickas, *J. High Energy Phys.* **0209** (2002) 038.
- [32] K. Chan, U. Chattopadhyay and P. Nath, *Phys. Rev. D* **58** (1998) 096004.
- [33] J. Feng, K. Matchev and T. Moroi, *Phys. Rev. Lett.* **84** (2000) 2322 and *Phys. Rev. D* **61** (2000) 075005.
- [34] S. Abdullin, A. Khanov and N. Stepanov, CMSJET, CMS TN/94-180 (2002).
- [35] H. Baer, C. Balázs and A. Belyaev, *J. High Energy Phys.* **0203** (2002) 042 and [hep-ph/0211213](#); see also H. Baer and M. Brhlik, *Phys. Rev. D* **53** (1996) 597.
- [36] P. Gondolo and G. Gelmini, *Nucl. Phys. B* **360** (1991) 145; J. Edsjö and P. Gondolo, *Phys. Rev. D* **56** (1997) 1879.
- [37] K. Abe *et al.* (Belle Collaboration), *Phys. Lett. B* **511** (2001) 151.
- [38] D. Cronin-Hennessy *et al.* (CLEO Collaboration), *Phys. Rev. Lett.* **87** (2001) 251808.
- [39] R. Barate *et al.* (Alephe Collaboration), *Phys. Lett. B* **429** (1998) 169.
- [40] H. Baer and M. Brhlik, *Phys. Rev. D* **55** (1997) 3201; H. Baer, M. Brhlik, D. Castaño and X. Tata, *Phys. Rev. D* **58** (1998) 015007.
- [41] G. Degrassi, P. Gambino and G. Giudice, *J. High Energy Phys.* **0012** (2000) 009. M. Carena, D. Garcia, U. Nierste and C. Wagner, *Phys. Lett. B* **499** (2001) 141.
- [42] G. W. Bennett *et al.* [Muon g-2 Collaboration], *Phys. Rev. Lett.* **89**, 101804 (2002) [Erratum-ibid. **89**, 129903 (2002)].

- [43] M. Knecht and A. Nyffeler, *Phys. Rev.* **D 65** (2002) 073034; M. Knecht, A. Nyffeler, M. Perrottet and E. De Rafael, *Phys. Rev. Lett.* **88** (2002) 071802; M. Hayakawa and T. Kinoshita, [hep-ph/0112102](#); I. Blokland, A. Czarnecki and K. Melnikov, *Phys. Rev. Lett.* **88** (2002) 071803; A. Nyffeler, [hep-ph/0209329](#).
- [44] K. Melnikov, *Int. J. Mod. Phys.* **A 16** (2001) 4591 (His updated analysis of the SM value of δa_μ was presented at the High Energy Physics Seminar, University of Hawaii, March 2002); F. Jegerlehner, [hep-ph/0104304](#); K. Hagiwara, A. D. Martin, D. Nomura and T. Teubner, [hep-ph/0209187](#).
- [45] M. Davier, S. Eidelman, A. Hocker and Z. Zhang, *Eur. Phys. J.* **C 27** (2003) 497.
- [46] H. Baer, C. Balázs, A. Belyaev, J. K. Mizukoshi, X. Tata and Y. Wang, *J. High Energy Phys.* **0207** (2002) 050 and [hep-ph/0210441](#).
- [47] S. Narison, [hep-ph/0303004](#).
- [48] H. Baer, C. Balázs, J. Ferrandis and X. Tata, *Phys. Rev.* **D 64** (2001) 035004.
- [49] F. Abe *et al.*, (CDF Collaboration), *Phys. Rev.* **D 57** (1998) 3811.
- [50] S. Rai Choudhury and N. Gaur, *Phys. Lett.* **B 451** (1998) 86; K. Babu and C. Kolda, *Phys. Rev. Lett.* **84** (2000) 228; A. Dedes, H. Dreiner and U. Nierste, *Phys. Rev. Lett.* **87** (2001) 251804; R. Arnowitt, B. Dutta, T. Kamon and M. Tanaka, *Phys. Lett.* **B 538** (2002) 121; J. K. Mizukoshi, X. Tata and Y. Wang, *Phys. Rev.* **D 66** (2002) 115003.
- [51] H. Baer and C. Balázs, [hep-ph/0303114](#).
- [52] J. Ellis, T. Falk, K. Olive and M. Srednicki, *Astropart. Phys.* **13** (2000) 181.
- [53] H. Baer and M. Brhlik, *Phys. Rev.* **D 57** (1998) 567.
- [54] H. Baer, M. Brhlik, M. Diaz, J. Ferrandis, P. Mercadante, P. Quintana and X. Tata, *Phys. Rev.* **D 63** (2001) 015007; J. Ellis, T. Falk, G. Ganis, K. Olive and M. Srednicki, *Phys. Lett.* **B 510** (2001) 236.
- [55] J. Feng, K. Matchev and F. Wilczek, *Phys. Lett.* **B 482** (2000) 388 and *Phys. Rev.* **D 63** (2001) 045024.
- [56] K. Griest and D. Seckel, *Phys. Rev.* **D 43** (1991) 3191.